Huntingtin-interacting protein family members have a conserved pro-viral function from *Caenorhabditis elegans* to humans

Hongbing Jiang[a,b,1,2], Luis Enrique Sandoval Del Prado[a,b,1], Christian Leung[a,b], and David Wang[a,b,2]

[a]Department of Molecular Microbiology, School of Medicine, Washington University in St. Louis, St. Louis, MO 63110; and [b]Department of Pathology & Immunology, School of Medicine, Washington University in St. Louis, St. Louis, MO 63110

Edited by James R. Priess, Fred Hutchinson Cancer Research Center, Seattle, WA, and approved July 30, 2020 (received for review April 11, 2020)

Huntingtin-interacting protein family members are evolutionarily conserved from yeast to humans, and they are known to be key factors in clathrin-mediated endocytosis. Here we identified the *Caenorhabditis elegans* protein huntingtin-interacting protein-related 1 (HIPR-1) as a host factor essential for Orsay virus infection of *C. elegans*. Ablation of HIPR-1 resulted in a greater than 10,000-fold reduction in viral RNA, which could be rescued by ectopic expression of HIPR-1. Viral RNA replication from an endogenous transgene replicon system was not affected by lack of HIPR-1, suggesting that HIPR-1 plays a role during an early, prereplication virus life-cycle stage. Ectopic expression of HIPR-1 mutants demonstrated that neither the clathrin light chain-binding domain nor the clathrin heavy chain-binding motif were needed for virus infection, whereas the inositol phospholipid-binding and F-actin–binding domains were essential. In human cell culture, deletion of the human HIP orthologs HIP1 and HIP1R led to decreased infection by Coxsackie B3 virus. Finally, ectopic expression of a chimeric HIPR-1 harboring the human HIP1 ANTH (AP180 N-terminal homology) domain rescued Orsay infection in *C. elegans*, demonstrating conservation of its function through evolution. Collectively, these findings further our knowledge of cellular factors impacting viral infection in *C. elegans* and humans.

HIPR-1 | Orsay virus | HIP1 | HIP1R | Coxsackie B3 virus

The identification of novel cellular factors that promote viral infection is key to advancing our understanding of the viral life cycle, and it has the potential to yield new therapeutic targets. The multicellular model organism *Caenorhabditis elegans* is naturally infected by Orsay virus, a positive-sense, nonenveloped RNA virus (1). This infection system has recently been utilized to identify several novel host factors that are essential for Orsay virus infection (2, 3). Through an unbiased forward genetic screen, the genes *sid-3*, *viro-2*, and *drl-1* were previously identified as host factors essential at an early stage of the Orsay virus life cycle (2, 3). This genetic screen utilized the *jyIs8;rde-1(ne219)* reporter strain, which expresses green fluorescent protein (GFP) under control of the virus-inducible gene promoter *pals-5* (2). In the *rde-1* mutant genetic background, which renders these animals hypersensitive to Orsay virus, virus infection typically leads to GFP expression in greater than 99% of animals. In this screen, following chemical mutagenesis, mutants that fail to express GFP fluorescence are selected (2). *C. elegans nck-1* is an additional critical factor for Orsay virus infection identified through an RNA interference (RNAi)-based reverse genetic screen targeting host factors interacting with the mammalian orthologs of *sid-3* and *viro-2* (2). Moreover, the human orthologs of *sid-3*, *viro-2*, and *nck-1* (*TNK2*, *WASP*, and *NCK1*, respectively) form a pathway that is important for infection by multiple viruses in the family *Picornaviridae* (3). In total, these studies establish that key pro-viral genes discovered in *C. elegans* may have evolutionarily conserved functions in mammals.

C. elegans huntingtin-interacting protein-related 1 (HIPR-1) belongs to the huntingtin-interacting protein (4) family, members of which have been studied in yeast and mammals. HIP-family proteins have a common domain architecture which includes an inositol phospholipid-binding AP180 N-terminal homology domain (ANTH) (5), a clathrin heavy chain-binding motif adjacent to a central clathrin light chain-binding coiled-coil (CC) domain, and a talin-HIP1/R/Sla2p actin-tethering C-terminal homology (THATCH) domain, which are thought to link the F-actin cytoskeleton and the clathrin-mediated endocytosis pathways (6–12). Biochemical and genetic evidence demonstrate that yeast and human HIP-family genes bind and colocalize with clathrin endocytic machinery during endocytosis, and that deletion of the yeast HIP-family member Sla2p or knockdown of the human HIP1R protein results in defects in clathrin-mediated endocytosis (6–12). However, HIPR-1's biological role in *C. elegans* has not been well-studied. *C. elegans* HIPR-1 is predicted by homology to have all of the canonical domains characteristic of HIP-family members, although no functional studies of these domains have been reported. HIPR-1 modulates presynaptic activity and the abundance of the synaptic vesicle fusion regulator synaptobrevin (13). In addition, a genome-wide RNAi screen suggests that HIPR-1 may be a regulator of the apical membrane peptide transporter PEPT-1 (14).

C. elegans HIPR-1 shares 33 and 34% amino acid identity with two human paralogs, HIP1 and HIP1R, respectively. The human HIP1 and HIP1R share 48% amino acid sequence identity with

Significance

Understanding host–virus interaction mechanisms is critical to identify novel drug targets for development of antiviral therapeutics. The *C. elegans*–Orsay virus infection system offers an innovative approach for discovering host factors required for virus infection. The *hipr-1* gene was determined to be essential in *C. elegans* for Orsay virus infection at an early stage of the virus life cycle. Studies of its orthologs in human cell culture determined that both HIP1 and HIP1R are important for Coxsackie B3 virus infection, highlighting the evolutionarily conserved role of HIP-family proteins in virus infection from nematodes to humans.

Author contributions: H.J., L.E.S.D.P., and D.W. designed research; H.J., L.E.S.D.P., C.L., and D.W. performed research; H.J., L.E.S.D.P., C.L., and D.W. contributed new reagents/analytic tools; H.J., L.E.S.D.P., C.L., and D.W. analyzed data; and H.J., L.E.S.D.P., and D.W. wrote the paper.

The authors declare no competing interest.

This article is a PNAS Direct Submission.

[1]H.J. and L.E.S.D.P. contributed equally to this work.

[2]To whom correspondence may be addressed. Email: hongbingjiang@wustl.edu or davewang@wustl.edu.

This article contains supporting information online at https://www.pnas.org/lookup/suppl/doi:10.1073/pnas.2006914117/-/DCSupplemental.

First published August 24, 2020.

each other (15). *C. elegans* HIPR-1 is more distantly related to its yeast ortholog Sla2p (15). Mice deficient in HIP1R exhibit viable and fertile (16), although one study identified a gastric parietal defect associated with transformation and hypertrophy of the glandular epithelium (17). HIP1-deficient mice, on the other hand, exhibit testicular degeneration, spinal defects, hematopoietic abnormalities, and cataracts (18, 19); in a separate study, an additional defect in AMPA receptor internalization in primary neurons was reported while hematopoiesis was normal (20). Mice deficient in both HIP1 and HIP1R exhibited aggravated spinal abnormalities and dwarfism, suggesting existence of a compensatory role of HIP1 and HIP1R (21). HIP proteins may be more functionally diverse than previously described, as studies in human cell culture have also suggested human HIP proteins may play a role in other cellular pathways such as androgen receptor transcription and apoptosis (22, 23). Only a few studies have investigated the potential role of mammalian HIP1 and HIP1R in virus infection (24–26). In the context of small interfering RNA (siRNA) screens, HIP1R has been reported as an important host factor for infection by Venezuelan equine encephalitis virus (26), while both HIP1 and HIP1R have been reported as important factors for hepatitis C virus, polio virus, and Coxsackie B3 virus (CVB3) infection (24, 25). However, little is known mechanistically about how these proteins promote virus infection.

Here we characterize a function of HIPR-1 as a host factor essential for Orsay virus infection. Its pro-viral function was dependent upon both its ANTH and THATCH domains but not its clathrin-binding domains. We demonstrated that the ANTH domain function is conserved from *C. elegans* to humans, as the human ANTH domain could replace the *C. elegans* ANTH domain. Deletion of the mammalian orthologs HIP1 and HIP1R in human cells led to reduced infection of CVB3, which further demonstrates the evolutionarily conserved pro-viral role this family plays. Collectively, this study provides insights into the mechanism of HIP proteins in virus infection, which appears to be clathrin binding-independent.

Results

In Vivo Mutagenesis Screen for Mutants Resistant to Orsay Virus Infection. To discover new host factors that Orsay virus relies upon for infection, an EMS (ethylmethanesulfonate) chemical mutagenesis screen was performed on ∼2,000 haploid genomes in the WUM28 *jyIs8;rde-1(ne219)* worm reporter strain as previously described (2) (*SI Appendix*, *Materials and Methods*). Two Viro (virus-induced reporter off) mutant strains, Viro-5 and Viro-6, demonstrated a defect in GFP expression upon Orsay virus challenge at 3 d post infection (dpi) (Fig. 1*A*). However, when these mutants were challenged with *Nematocida parisii*, a natural fungal pathogen of *C. elegans* that also activates the GFP transcriptional reporter, both Viro-5 and Viro-6 displayed wild-type levels of GFP in response to fungal infection, demonstrating a virus-specific defect in GFP activation (Fig. 1*A*). Orsay RNA replication was quantified by quantitative real-time RT-PCR at 3 dpi and revealed a reduction of greater than 10,000-fold in both Viro-5 and Viro-6 mutants compared with the unmutagenized parental strain (Fig. 1*B*).

To determine whether Viro-5 and Viro-6 fell into the same genetic complementation group, they were crossed with each other. Viro-5 and Viro-6 fell into the same complementation group, suggesting they harbor independent mutant alleles of the same gene (*SI Appendix*, Fig. S1).

Two Independent Mutant Alleles of *hipr-1* Are Responsible for the Virus Resistance Phenotype. Two independent approaches were used in parallel to map the phenotype-causing mutations in Viro-5 and Viro-6. In the first approach, F2 bulk segregant analysis was performed on Viro-6 as previously described (2, 27) (*SI*

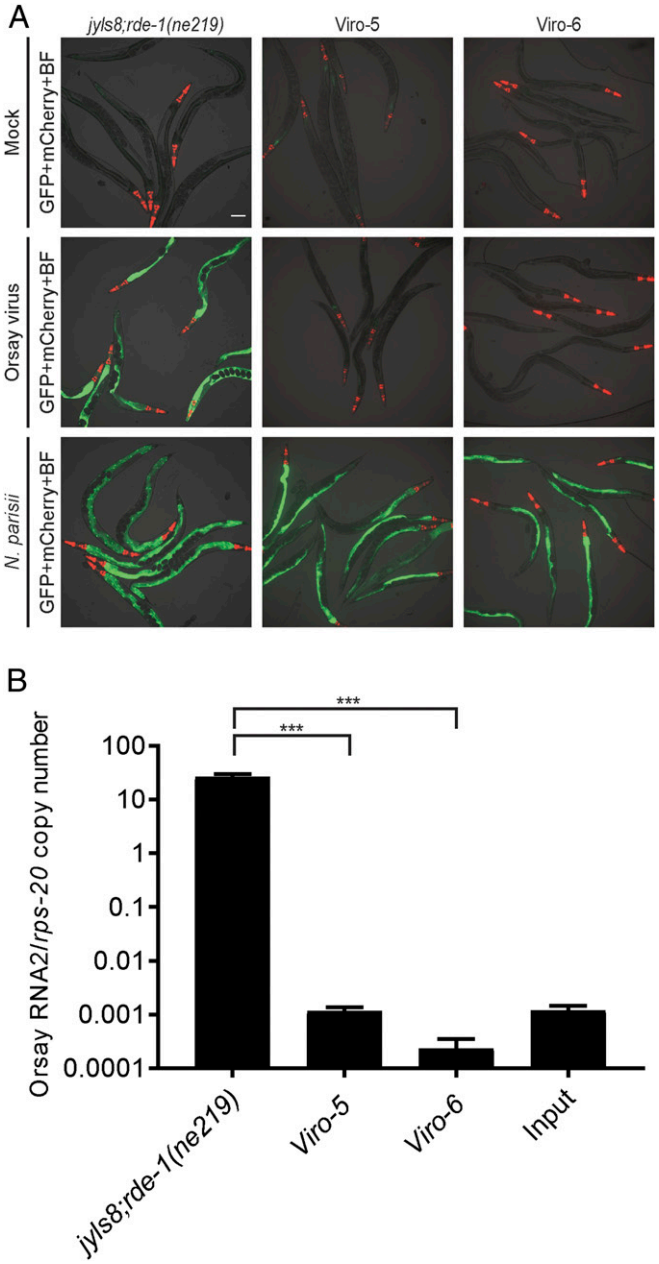

Fig. 1. Chemical mutagenesis screen identified mutant strains with a defect in GFP expression and Orsay viral RNA replication. (*A*) GFP reporter expression of Viro mutants infected with Orsay virus or *N. parisii* at 3 dpi. *Pmyo2::mCherry* is a transgenic marker. (Scale bar, 100 μm.) BF, bright field. (*B*) Orsay virus RNA2 levels quantified by real-time qRT-PCR at 3 dpi. The means and SDs for three replicates representative of at least two independent biological experiments are shown. Statistically significant differences were determined by Student's *t* test. ***$P < 0.001$.

Appendix, *Materials and Methods*). In the second approach, the original Viro-5 and Viro-6 mutant strains were each subjected to whole-genome sequencing (*SI Appendix*, *Materials and Methods*). Both approaches yielded *hipr-1* as the candidate causal gene. *hipr-1* in Viro-5 harbored a candidate G-to-A nonsense mutation that converts an arginine at position 515 to a premature stop, and *hipr-1* in Viro-6 contained a candidate G-to-A missense mutation that results in a G773E amino acid substitution (Fig. 2*A*).

To determine whether *hipr-1* was the causal gene for the Viro-5 and Viro-6 phenotypes, we tested the impact of RNAi knockdown

MICROBIOLOGY

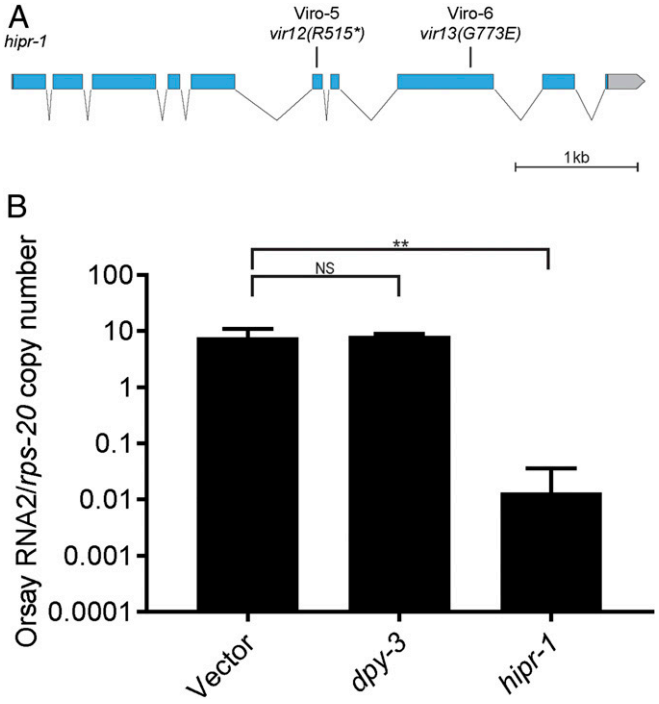

Fig. 2. *hipr-1* mutant alleles and RNAi knockdown. (*A*) A *hipr-1* genomic structure schematic showing the position and identity of *hipr-1* mutant alleles in Viro-5 and Viro-6. The coding region is represented in blue, untranslated region sequences are in gray, and introns are represented as lines. *, stop codon. (*B*) qRT-PCR of Orsay virus RNA2 levels 2 dpi of Orsay virus infection of *drh-1* animals fed with RNAi against targeted genes, nontargeted genes, or empty vector. The means and SDs for three replicates representative of at least two independent biological experiments are shown. Statistically significant differences were determined by one-way ANOVA with a statistical difference identified between the empty vector and *hipr-1* by Dunnett's multiple-comparison test. $^{**}P < 0.01$; NS, not significant ($P > 0.05$).

of *hipr-1* on Orsay virus RNA levels. RNAi knockdown of *hipr-1* was performed in the *drh-1* mutant background. The *drh-1* mutant strain is competent for exogenous feeding RNAi yet is hypersensitive to Orsay virus infection due to a defect in antiviral RNAi; this strain provides a larger dynamic range to measure changes in Orsay virus RNA levels than the wild-type N2 (2). At 2 dpi, Orsay virus RNA levels were reduced by over 1,000-fold compared with the empty vector and nonrelevant gene control *dpy-3*, supporting *hipr-1* as the causal gene (Fig. 2*B*). As an independent validation, we ectopically expressed the genomic locus of *hipr-1* under the control of the constitutively active *sur-5* gene promoter in both Viro-5 and Viro-6. At 3 dpi, wild-type levels of GFP expression and Orsay RNA replication were observed in both transgenic strains, collectively demonstrating that the mutations in *hipr-1* were responsible for the Viro phenotypes (*SI Appendix*, Fig. S2 *A* and *B*). Thus, Viro-5 and Viro-6 will be referred to as *hipr-1(vir12)* and *hipr-1(vir13)*, respectively, hereafter.

HIPR-1 Inositol Phospholipid- and F-Actin–Binding Domains Are Required for Orsay Virus Infection. To explore which HIPR-1 domains are important for Orsay virus infection, the following HIPR-1 expression constructs harboring deletions were generated (Fig. 3 *A* and *B*): the HIPR-1 ANTH deletion (ΔANTH), which is predicted to abolish binding to inositol phospholipids (9, 10); the HIPR-1 coiled-coil domain (ΔCC), which is predicted to abolish binding to the clathrin light chain (28, 29); the HIPR-1 THATCH deletion (ΔTHATCH), which is predicted to abolish binding to F-actin (30, 31); a deletion of the clathrin heavy chain-binding motif LLNLA (ΔCHC), which is predicted to abolish binding to the clathrin heavy chain, as this consists of the type I consensus clathrin box (LL/I)(D/E/N)(L/F)(D/E) (32, 33); and a double deletion (ΔCHCΔCC) of both the clathrin heavy chain-binding motif and the clathrin light chain-binding coiled-coil domain. All mutations were generated in the HIPR-1 expression construct described above fused with mCherry as an expression

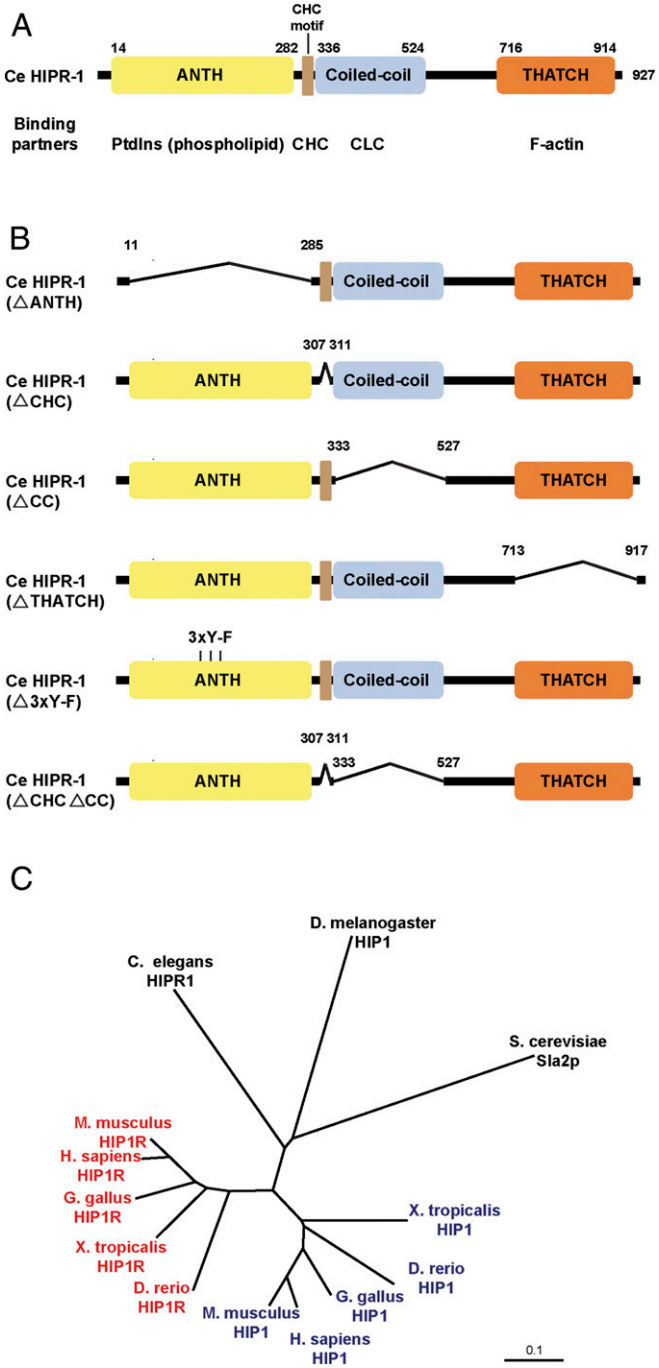

Fig. 3. HIPR-1 domain structure and evolutionary conservation of HIP proteins. (*A*) A schematic depicting HIPR-1's three predicted evolutionarily conserved domains and clathrin heavy chain-binding type I consensus clathrin box. (*B*) A schematic depicting the deletions or mutations that were introduced into the HIPR-1 expression construct, which were all mCherry-tagged at the C terminus for visualization of expression. Numbers represent the amino acids deleted. (*C*) Neighbor-joining phylogenetic tree for HIP proteins across species. The scale bar represents amino acid substitution.

marker, and quantification of the mCherry signal showed all strains were expressed at comparable levels as the wild-type HIPR-1::mCherry strain or higher (*SI Appendix*, Fig. S3). Ectopic expression of wild-type HIPR-1::mCherry, HIPR-1::mCherry(ΔCHC), HIPR-1::mCherry(ΔCC), or HIPR-1::mCherry(ΔCHCΔCC) in *hipr-1(vir12)* was sufficient to rescue both GFP expression and Orsay virus RNA replication at 3 dpi, suggesting both HIPR-1's clathrin light chain-binding domain and clathrin heavy chain-binding motif were dispensable for Orsay virus infection (Fig. 4). By contrast, ectopic expression of HIPR-1::mCherry(ΔANTH) or HIPR-1::mCherry(ΔTHATCH) in *hipr-1(vir12)* mutants failed to rescue GFP expression and Orsay virus RNA replication at 3 dpi, implicating inositol phospholipid and F-actin binding as key functions of HIPR-1 in virus infection in *C. elegans* (Fig. 4 *A* and *B*).

As four tyrosines in the human HIP1 ortholog were previously reported to be phosphorylated by the receptor tyrosine kinase epidermal growth factor receptor (23) and this phosphorylation was important for cell survival, we investigated whether phosphorylation of the analogous tyrosines in *C. elegans* HIPR-1 affects Orsay virus infection. As three of these tyrosines were conserved in HIPR-1, we engineered a triple tyrosine-to-phenylalanine (Y-F) nonphosphorylatable mutant form of HIPR-1 (Fig. 3*B*). Ectopic expression of HIPR-1(3xY-F) in *hipr-1(vir12)* was sufficient to rescue both GFP expression and Orsay virus RNA replication at 3 dpi (Fig. 4 *A* and *B*), suggesting that phosphorylation (or lack thereof) of these three tyrosines in HIPR-1 does not impact Orsay virus infection.

HIPR-1 Affects Orsay Virus at an Early, Prereplication Step of Infection. To investigate which stage of the Orsay virus life cycle HIPR-1 affects, an endogenous inducible viral RNA transgene replicon system was generated in *hipr-1(vir12)* as previously described (2). These transgenic strains carry an extrachromosomal

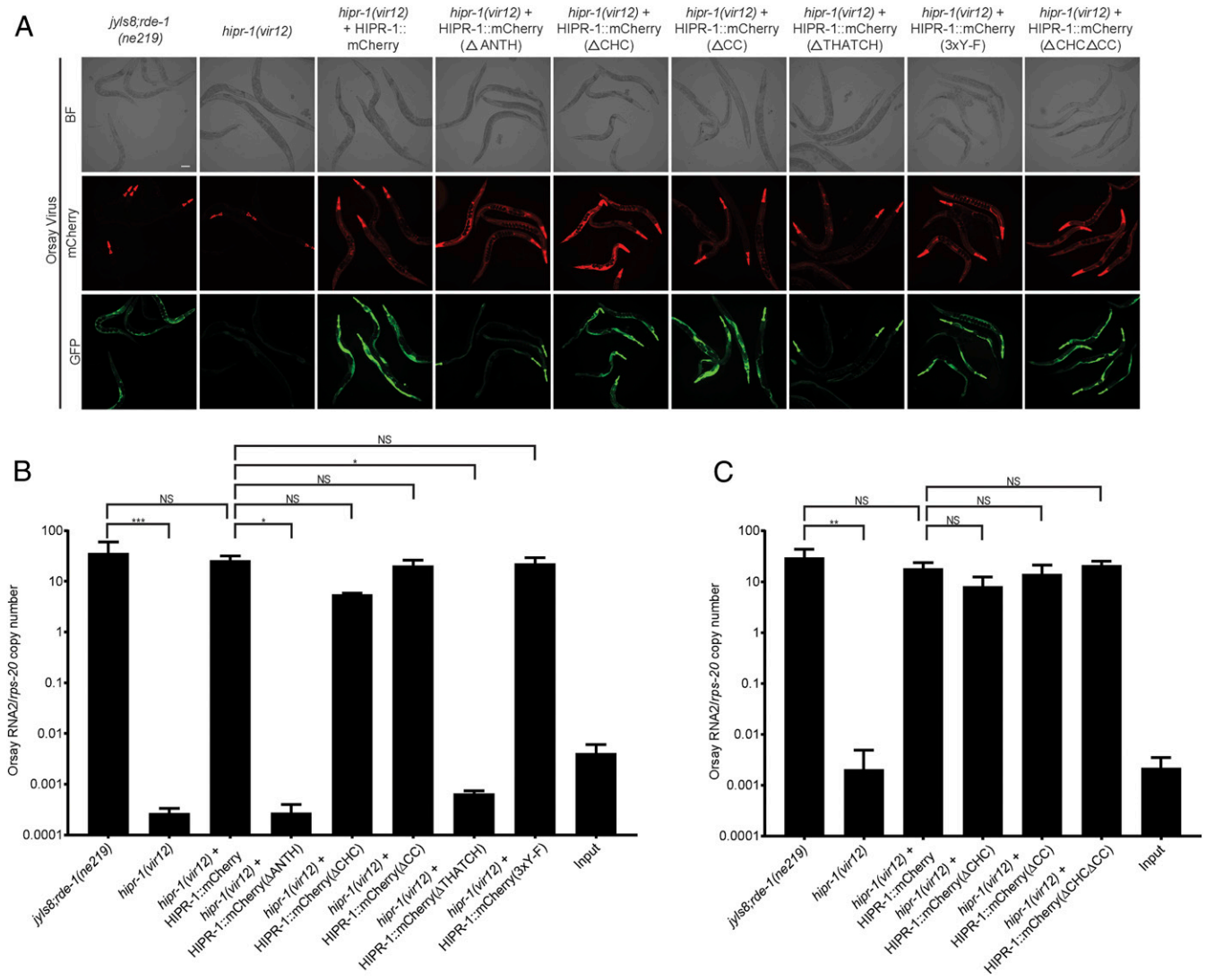

Fig. 4. GFP reporter expression and virus RNA replication in *hipr-1(vir12)* transgenic animals overexpressing various HIPR-1::mCherry constructs. (*A*) Intestinal GFP expression at 3 dpi of transgenic animals infected with Orsay virus. The *Pmyo2::YFP* plasmid was coinjected as a transgenic marker and is observed as GFP in the pharynx of transgenic animals. (Scale bar, 100 μm.) (*B*) Orsay virus RNA2 levels at 3 dpi in transgenic *hipr-1(vir12)* animals overexpressing HIPR-1::mCherry constructs containing a variety of mutations. (*C*) Orsay virus RNA2 levels at 3 dpi in transgenic *hipr-1(vir12)* animals overexpressing HIPR-1::mCherry constructs lacking the clathrin heavy chain motif, coiled-coil domain, or both. The means and SDs for three replicates representative of at least two independent biological experiments are shown. Statistically significant differences were determined by one-way ANOVA with a statistical difference identified between three post hoc comparisons analyzed by Sidak's multiple-comparison test. $*P < 0.05$, $**P < 0.01$, $***P < 0.001$.

array of plasmids expressing, under control of the heat-inducible promoter from *hsp-16* genes, either the wild-type Orsay virus RNA1 segment or a mutant RNA1 segment harboring an inactivating mutation (D601A) in the RNA-dependent RNA polymerase. The latter strain acts as a control to define levels of DNA-templated transcription of the viral transgene. Heat induction of *hipr-1(vir12)* transgenic strains carrying the wild-type viral RNA transgene displayed intestinal GFP expression and Orsay virus RNA1 replication comparable to levels observed in the wild-type strain *jyIs8;rde-1(ne219)* harboring the same construct, while transgenic strains expressing the polymerase-dead mutant did not induce GFP expression or RNA1 replication (Fig. 5). Together, these results demonstrated that Orsay virus replication initiated from an endogenous transgene is not dependent on HIPR-1 and, therefore, HIPR-1 acts at early steps upstream of Orsay virus replication.

HIP1 and HIP1R, the Mammalian Orthologs of *C. elegans* HIPR-1, Are Important for CVB3 Infection. Because HIP-family proteins are evolutionarily conserved from yeast to humans (Fig. 3*C*), we evaluated the roles of HIP1 and HIP1R in mammalian virus infection. Both HIP1 and HIP1R knockout cells were generated by CRISPR-Cas9 genome editing in A549 cells, a lung epithelial carcinoma cell line (Fig. 6 *A* and *D*). Single-step infection by CVB3 at a multiplicity of infection (MOI) of 1 showed ~40% reduction of infection in HIP1 knockout cells and ~50% reduction of infection in HIP1R knockout cells compared with control cells as quantified by flow cytometry analysis of CVB3-positive cells (Fig. 6 *B* and *E*). In a multistep growth curve analysis, a 10-fold reduction was seen at late time points of virus infection in HIP1 knockout and HIP1R knockout cells (Fig. 6 *C* and *F*). Although both HIP1 and HIP1R are thought to be important in endocytosis, using fluorescently labeled transferrin, a canonical cargo for clathrin-mediated endocytosis, analysis by flow cytometry demonstrated no defect in transferrin uptake in any of the knockout cells (*SI Appendix*, Fig. S4), which is consistent with previously reported transferrin endocytosis in HIP1 and HIP1R knockout mouse embryonic fibroblast cells (16, 21).

Ectopic lentivirus-mediated overexpression of HIP1 or HIP1R in the corresponding knockout cells rescued CVB3 infection to control cell levels (Fig. 6 *J–M*). To evaluate whether HIP1 and HIP1R had synergistic roles in virus infection, a HIP1 and HIP1R double-knockout A549 cell line was generated using the same targeting single-guide RNAs (sgRNAs) (Fig. 6*G*). Infection of the double mutant by CVB3 resulted in similar levels of reduction as either single mutant (Fig. 6*H*). Similarly, a multistep growth analysis showed that HIP1 and HIP1R double-knockout cells had similar 10-fold reduction of virus production as compared with the control cells (Fig. 6*I*). The lack of an additive effect of the HIP1/HIP1R knockout suggests that the two genes might function in the same pathway.

HIP1 is known to bind to the N-terminal sequence of huntingtin (34, 35). Thus, we tested whether overexpressing the huntingtin N-terminal sequence would influence CVB3 infection. Lentivirus-mediated expression of the 541-amino acid N terminus of huntingtin in naïve A549 cells decreased infection by CVB3 as compared with control cells transduced to express firefly luciferase (*SI Appendix*, Fig. S5).

To determine if CVB3 dependence on HIP1 and HIP1R was specific to the A549 cell line, we evaluated HIP1, HIP1R, and HIP/HIP1R knockouts in the Hap1 cell line, a hematopoietic haploid cell line. Infection by CVB3 showed a similar reduction phenotype in HIP1, HIP1R, and HIP1/HIP1R double knockouts (*SI Appendix*, Fig. S6), demonstrating that their role in promoting CVB3 infection is also conserved across multiple cell types.

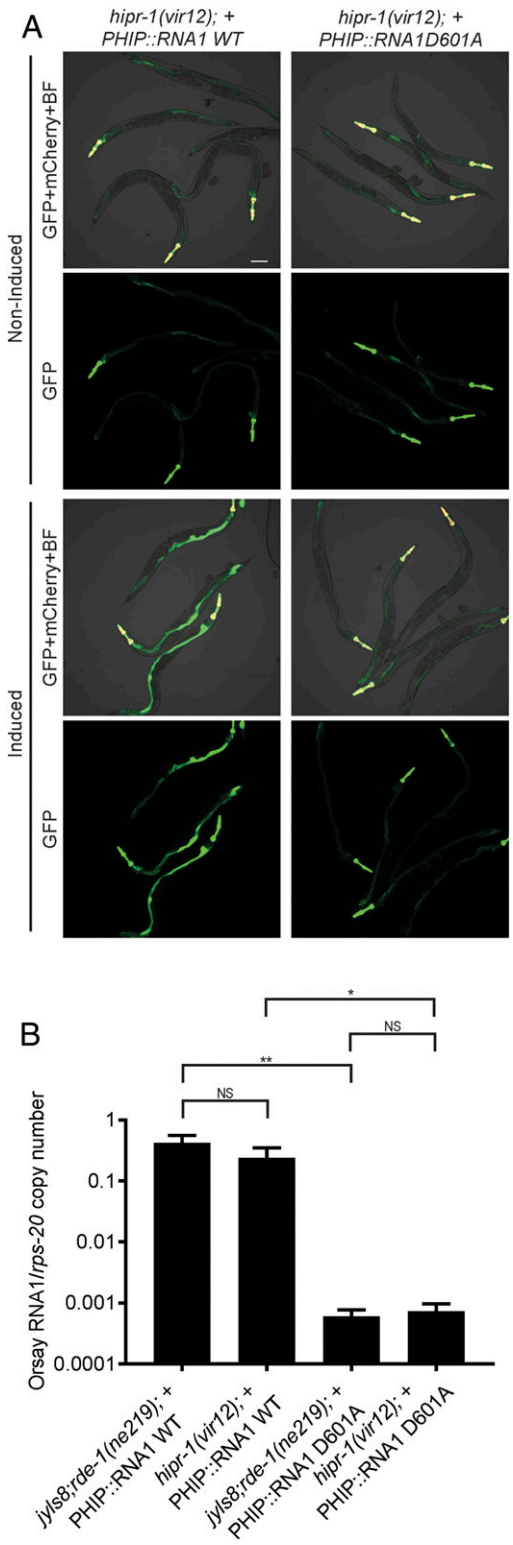

Fig. 5. Impact of *hipr-1* on Orsay virus RNA replication induced from the RNA1 transgene. (*A*) GFP expression of strains carrying wild-type or polymerase-dead mutant Orsay virus RNA1 under a heat-inducible promoter 3 d after heat shock. A *Pmyo2::YFP* plasmid was coinjected as a transgenic marker and is observed as GFP in the pharynx of transgenic animals. (Scale bar, 100 μm.) PHIP, heat-inducible promoter; WT, wild type. (*B*) Quantification of Orsay virus RNA1 replication 3 d after heat shock by real-time qRT-PCR. The means and SDs for three replicates representative of at least two independent biological experiments are shown. Statistically significant differences were determined by Student's *t* test. $*P < 0.05$, $**P < 0.01$.

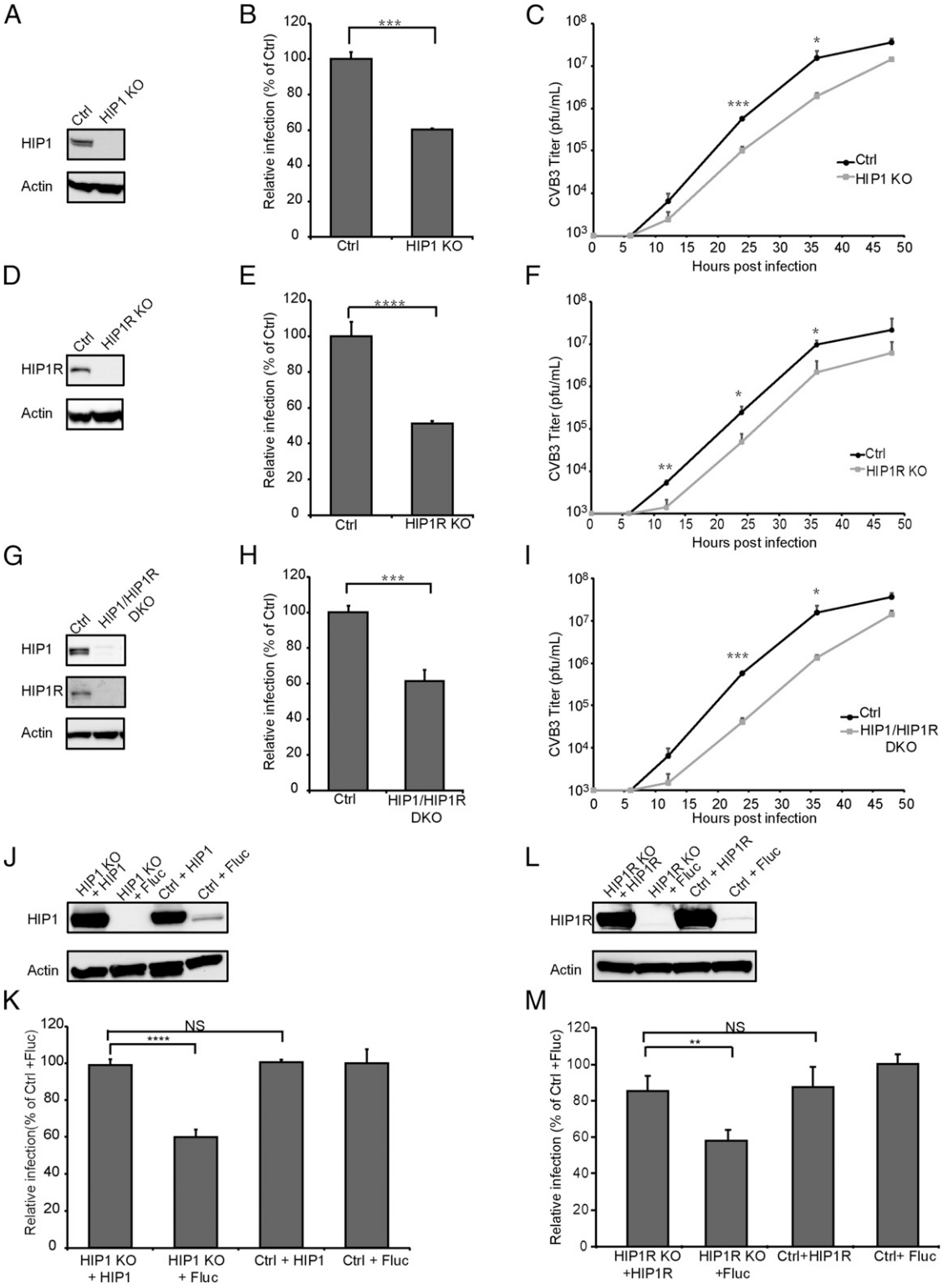

Fig. 6. HIP1 and HIP1R are important for CVB3 infection. (*A*, *D*, *G*, *J*, and *L*) HIP1 and HIP1R expression in knockout and rescued cells detected by Western blot. (*B*, *E*, *H*, *K*, and *M*) FACS quantification of CVB3 infection on HIP1 and HIP1R knockout and rescued cells 8 h post inoculation. Fluc, firefly luciferase. (*C*, *F*, and *I*) Multistep growth analysis of CVB3 on HIP1, HIP1R knockout, and double-knockout (DKO) cells. pfu, plaque-forming unit. The means and SDs for three replicates representative of at least two independent biological experiments are shown. Statistically significant differences were determined by Student's *t* test. $*P < 0.05$, $**P < 0.01$, $***P < 0.001$, $****P < 0.0001$.

The Human HIP1 ANTH Domain Is Functional in *C. elegans*. To determine if the human HIP1 ANTH domain is functional in *C. elegans*, we ectopically expressed codon-optimized human HIP1 ANTH domain chimeric protein in the *C. elegans* HIPR-1 expression backbone by swapping in the human HIP1 ANTH domain (Fig. 7*A*). Ectopic expression in *hipr-1(vir12)* of the construct carrying the human ANTH domain rescued both virus-induced GFP expression and the Orsay virus RNA replication phenotypes (Fig. 7 *B* and *C*). These data demonstrate that the human ANTH domain of HIP1 is functional in *C. elegans*.

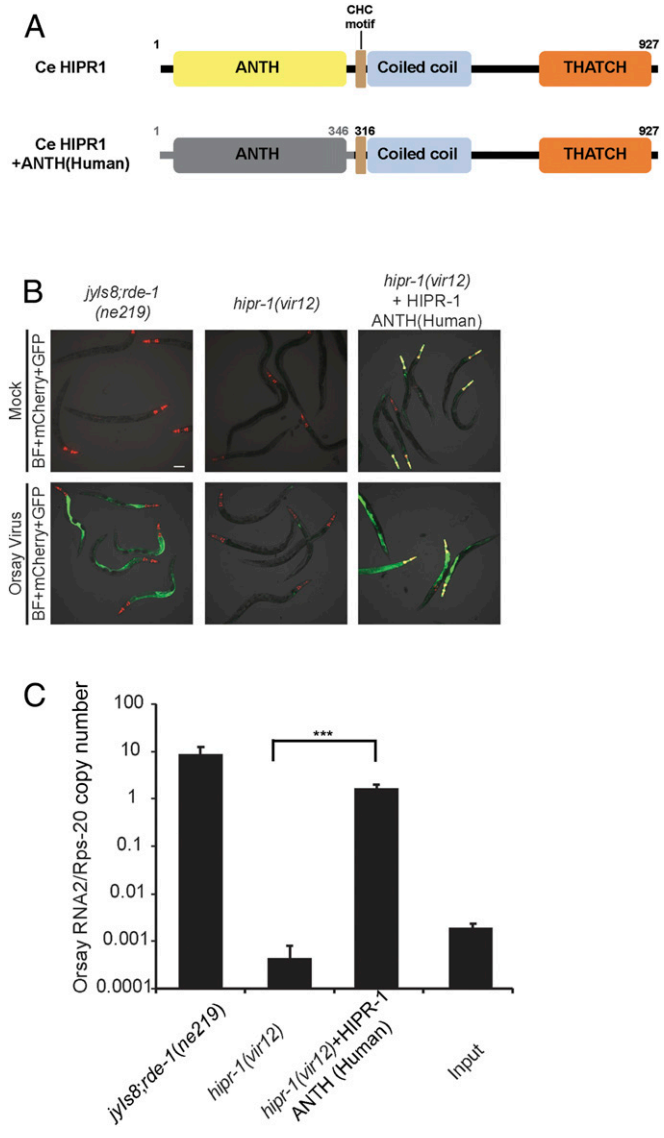

Fig. 7. Domain swapping between *C. elegans* HIPR-1 and human HIP1. (*A*) Domain structure for chimeric *C. elegans* HIPR-1 with the human HIP1 ANTH domain. The gray numbers represent the amino acids introduced from the human HIP1 ANTH for chimeric construction and the black numbers represent the *C. elegans* amino acid positions. (*B*) GFP reporter expression of Orsay virus infection in the *hipr-1(vir12)* strain ectopically expressing *C. elegans* HIPR-1 with the human ANTH domain. A *Pmyo2::YFP* plasmid was coinjected as a transgenic marker and is observed as GFP in the pharynx of transgenic animals. (Scale bar, 100 μm.) (*C*) Orsay virus RNA2 quantification in the *hipr-1(vir12)* strain ectopically expressing *C. elegans* HIPR-1 with the human ANTH domain. The means and SDs for three replicates representative of at least two independent biological experiments are shown. Statistically significant differences were determined by Student's *t* test. ***$P < 0.001$.

Discussion

There are only limited studies to date investigating the role of HIP-family proteins in virus infection. No studies have previously examined *C. elegans* HIPR-1 or its yeast ortholog, *Sla2p*, in the context of viral infection. The human ortholog HIP1R is a hit in an siRNA screen for Venezuelan equine encephalitis virus infection, and both HIP1 and HIP1R are hits in hepatitis C virus, poliovirus, and CVB3 infection screens. Although it has been suggested that these HIP proteins likely function in clathrin-mediated endocytosis to promote virus infection, the mechanism has not been investigated fully (24–26). In this study, we exploited the power of *C. elegans* forward genetic screens to define the essential role of HIPR-1 in Orsay virus infection. Moreover, we determined that HIPR-1's function is dependent on its inositol phospholipid- and F-actin–binding domains but independent of its clathrin light chain-binding domain and clathrin heavy chain-binding motif.

In human cells, we determined that both human orthologs of *C. elegans* HIPR-1, HIP1 and HIP1R, were important for CVB3 infection in cell culture, demonstrating the evolutionary conservation of HIP-family proteins in supporting virus infection from *C. elegans* to humans. In HIP1 and HIP1R double-knockout cells, the absence of an additive effect on virus growth suggests that HIP1 and HIP1R act in the same pathway to support virus infection. It is known that HIP1 and HIP1R can form both homodimers and heterodimers and this may be important for its endocytic function (36–38). Thus, one plausible explanation is that dimerization of HIP1 and HIP1R may play a role in promoting virus infection. Consistent with our data demonstrating that HIPR-1 in *C. elegans* acts in an early stage of Orsay virus infection, the ~50% reduction in CVB3-infected cells in single-step infection suggests that HIP1 and HIP1R are likely important for an early step of the virus life cyle. Further studies are required to determine whether these genes might also impact later stages of the virus life cycle.

The two *hipr-1* mutant alleles identified in this study phenocopy the viral replication and GFP induction defects observed in the previously identified essential *C. elegans* host gene mutant alleles *sid-3*, *viro-2*, and *nck-1* (2). As the human orthologs of *sid-3*, *viro-2*, and *nck-1* have since been demonstrated to function in a pathway (3), it is intriguing to speculate that *hipr-1* may also be part of this pathway. However, as all mutant alleles represent null function for Orsay virus infection in *C. elegans*, any genetic endeavor to reveal their relationship remains challenging in *C. elegans*.

HIPR-1's cellular function has not been well-defined in *C. elegans*. However, models for its yeast and human orthologs propose that HIP proteins are recruited to clathrin pits, where they bind the plasma membrane, F-actin, and clathrin to mediate initiation of endocytic vesicles (6, 8, 10). The domain analysis in this study demonstrated that *C. elegans* HIPR-1's inositol phospholipid- and F-actin–binding domains are essential for its function in Orsay virus infection, consistent with a model where HIPR-1 couples the plasma membrane and F-actin to mediate endocytosis. However, neither HIPR-1's clathrin heavy chain-binding motif nor its clathrin light chain-binding domain were necessary for Orsay virus infection, suggesting that HIPR-1's function may be clathrin-independent. An alternative possibility is that HIPR-1 indirectly binds to clathrin through a separate endocytic factor, as HIP proteins have been reported to bind to other endocytic factors, such as to clathrin adaptor protein 2 (AP2) in human cells and Sla1p in yeast (20, 39). While *C. elegans* HIPR-1 lacks the AP2 Asp-Pro-Phe (DPF)-binding motif and there is no Sla1p ortholog in *C. elegans*, there may be additional endocytic binding partners of HIPR-1. It is also plausible that HIPR-1 may be mediating clathrin-mediated endocytosis through a clathrin binding-independent mechanism.

The type of inositol phospholipids that *C. elegans* HIPR-1 binds to remains unknown. However, biochemical studies in the yeast ortholog Sla2p have previously reported that it binds to phosphatidylinositol (PtdIns)(4,5)P_2 lipids (9), which are primarily found at clathrin-coated pits at the cell surface and are important for recruiting key endocytic machinery (40, 41). Biochemical studies of the human orthologs HIP1 and HIP1R, in contrast, show that they preferentially bind to PtdIns(3,4)P_2, PtdIns(3,5)P_2, and, to a less extent, PtdIns(3)P (9), which are not enriched at the cell surface but instead in early and late endosomes, and play an important role in endosomal trafficking and protein sorting (42, 43). Together with the results from our chimeric HIPR-1 experiments, which demonstrated that the HIP1 ANTH domain was functional in *C. elegans*, it suggests the possibilities that *C. elegans* HIPR-1 may be acting at or after the internalization step of endocytosis during Orsay virus infection.

In conclusion, our genetic studies have identified HIP-family members as being evolutionarily conserved pro-viral host factors from *C. elegans* to humans. Domain analysis elucidated that the HIP protein's inositol phospholipid-binding and F-actin–binding abilities are critical for its pro-viral function in *C. elegans*, which appears to be clathrin binding-independent. Furthermore, this study established evidence of functional conservation between HIP-family member domains across evolution through a *C. elegans*–human chimeric protein. Collectively, these findings further highlight the power of *C. elegans* in identifying novel evolutionarily conserved host factors critical for virus infection, which can ultimately lead to attractive targets for antiviral therapeutics.

Materials and Methods

An extended description of the materials and methods used in this study is provided in *SI Appendix*, including the following: chemical mutagenesis screen, genetic mapping of the phenotype-causing mutations in Viro-5 and Viro-6, mCherry fluorescence quantification, transferrin uptake assay, N-terminal huntingtin expression, and CVB3 infection.

***C. elegans* Culture and Maintenance.** We obtained *C. elegans* strains WM27 *rde-1(ne219)* and RB2519 *drh-1(ok3495)* from the Caenorhabditis Genetics Center (CGC) and maintained them under standard laboratory culture conditions unless otherwise specified (Table 1). In summary, animals were fed *Escherichia coli* OP50 on nematode growth medium (NGM) plates in a 20 °C incubator and chunked every 3 to 4 d to a new NGM plate seeded with *E. coli* OP50.

Orsay Virus Preparation, Infection, and RNA Extraction. Orsay virus was prepared by large-scale liquid culture as described previously (2) and filtered through a 0.22-μm filter, and aliquots were stored at −80 °C. For all Orsay virus infection experiments, animals were bleached and then synchronized in M9 buffer in 15-mL conical tubes with constant rotation at room temperature for 16 h. In six-well plates with 20 μL *E. coli* OP50, 500 arrested larval stage 1 (L1) larvae were seeded. L1 larvae were allowed to recover for 20 h at 20 °C prior to infection. Orsay virus filtrate was thawed and brought to room temperature and then a 1:10 dilution was made with M9 buffer. For each well, 20 μL of virus filtrate was added to the middle of the bacterial lawn and the infection was incubated at 20 °C. At 3 dpi, animals were collected into 1.5-mL Eppendorf tubes by rinsing each well with 1 mL of M9 buffer and then spun down by spinning for 1 min at 3,000 rpm in a benchtop centrifuge. M9 supernatant was removed, 300 μL TRIzol reagent (Invitrogen) was added to the tubes, and they were frozen in liquid nitrogen. For Orsay virus infection assays an input control was included consisting of input virus that was incubated in an empty well for the duration of the experiment and subsequently mixed with an uninfected well of animals immediately prior to RNA extraction, to control for any degradation of the input virus in the absence of any replication. For each experiment, three replicate wells (technical replicates) were used for each infection condition, unless otherwise indicated. Total RNA from infected animals was extracted using Direct-zol RNA Miniprep (Zymo Research) purification according to the manufacturer's protocol and eluted into 30 μL of RNase/DNase-free water. For all *N. parisii* infection experiments, animals were bleached and then synchronized in M9 buffer in 15-mL conical tubes with constant rotation at room temperature for 16 h. In six-well plates with 20 μL *E. coli* OP50, 500 arrested L1 larvae were seeded. L1 larvae were allowed to recover for 20 h at 20 °C prior to infection. *N. parisii* spores were thawed and brought to room temperature and then a 1:10 dilution was made with M9 buffer. For each well, 20 μL of diluted *N. parisii* spores (10,000 spores per animal) was added to the middle of the bacterial lawn and the infection was incubated at 20 °C. At 3 dpi, animals were assayed for GFP fluorescence. For all of the infection experiments, at least two independent biological experiments (performed on different days) were performed.

***C. elegans* Feeding RNAi Knockdown.** Genes were knocked down by RNAi feeding as described previously (2). *E. coli* strain HT115 carrying double-strand RNA expression cassettes for genes of interest was induced using established conditions and then seeded into six-well NGM plates. *dpy-3* and *hipr-1* RNAi clones were from the Ahringer RNAi library (44). Twenty arrested L1 *drh-1* mutant animals were seeded into each well of a six-well plate. After 72 h of RNAi feeding, Orsay virus was added to the plates as described above. At 2 dpi the animals were collected, and 300 μL of TRIzol (Invitrogen) was added to each well for RNA extraction.

Orsay Virus Quantification by Real-Time qRT-PCR. RNA extracted from infected animals was subjected to one-step real-time qRT-PCR to quantify Orsay virus replication as previously described (2). The extracted RNA was diluted 1:100, and 5 μL was used in a TaqMan Fast Virus 1-Step qRT-PCR with primers GW303 and GW304 and probe Orsay_RNA2 (*SI Appendix*, Table S1) that target the Orsay RNA2 segment. Primers GW314 and GW315 and probe Orsay_RNA1 that target the Orsay virus RNA1 segment were used to quantify Orsay virus RNA1 abundance. To control for variation in the number of animals per well, Orsay virus RNA levels were normalized to an internal control gene, *rps-20*, which encodes a small ribosomal subunit S20 protein required for translation in *C. elegans*, using primers KC291 and KC292 and probe rps-20_e3-4. Absolute Orsay virus RNA2 and RNA1 and *C. elegans rps-20* copy number was determined by interpolation of a standard curve generated using serial dilutions of in vitro transcripts of Orsay virus RNA2 and RNA1 and *C. elegans rps-20*, respectively. The mean and SD for three replicate wells are shown for all experiments. Statistical testing was done by Student's *t* test or one-way ANOVA. Statistically significant comparisons are indicated as follows: ****$P < 0.0001$, ***$P < 0.001$, **$P < 0.01$, *$P < 0.05$; NS, not significant (with $P > 0.05$).

Forward Genetic Screen for Mutants That Fail to Activate GFP Expression following Orsay Virus Infection. The *jyIs8;rde-1* reporter strain was maintained on 10-cm plates seeded with 1.5 mL *E. coli* OP50. Animals were grown to a stage with a high proportion of L4 larvae and were then collected by rinsing the plates with water. Animals were then treated with 50 mM EMS for 4 h at 20 °C with constant rotation, washed with M9 buffer, and recovered on 10-cm plates for 6 h. Ten L4 P0 animals were transferred to 10 new NGM plates and allowed to lay about 10 F1 eggs each before being removed. F1 animals were washed away from plates after laying about 20 eggs for each animal. Hatched F2 animals were challenged with 800 μL of the standard virus filtrate dilution for infection and screened for Viro mutants. For complementation assays, eight males of one Viro mutant were crossed with two hermaphrodites of another Viro mutant to define the ability of their progeny to complement the Viro phenotypes.

Mapping the Causal Gene Mutation through F2 Bulk Segregant and CloudMap Analysis. As previously described (2), *hipr-1(vir13)* mutants were crossed with the WM27 *rde-1(ne219)* strain, and F1 progenies were chosen and transferred to six-well plates. After 2 d, the F2 progenies were infected with Orsay virus at the standard 1:10 dilution of the virus filtrate. At 3 dpi of the F1 plates, 72 F2 Viro animals were picked off F1 plates and transferred to six-well plates. F2 plates were replicated after 2 d of laying eggs. The original F2 plates were challenged again with Orsay virus, and both GFP expression and viral RNA replication phenotypes were tested at 3 dpi. Forty-two wells that yielded Viro animals and that yielded low RNA levels from replicated F2 plates were pooled, and genomic DNA from the pooled samples was extracted using a Qiagen genomic DNA preparation kit according to the manufacturer's protocol. DNA libraries were prepared using a Nextera library preparation kit (New England Biolabs) and then sequenced using Illumina MiSeq Standard. The raw sequence data were analyzed using the pipeline CloudMap for *C. elegans* gene mapping (27).

Table 1. Strains used in this study

Lab name	Strain name	Relevant genotype
WM27	*rde-1(ne219)*	*[rde-1(ne219)V]*
RB2519	*drh-1(ok3495)*	*[drh-1(ok3495)IV]*
WUM32	*jyIs8;rde-1(ne219); virEx20[PHIP::RNA1WT-1]*	*{virEx20[PHIP::OrsayRNA1WT-1; Pmyo-2::YFP]; jyIs8[Ppals-5::GFP;Pmyo-2::mCherry];rde-1(ne219) V}*
WUM33	*jyIs8;rde-1(ne219); virEx21[PHIP::RNA1D601A-1]*	*{virEx21[PHIP::OrsayRNA1D601A-1; Pmyo-2::YFP]; jyIs8[Ppals-5::GFP;Pmyo-2::mCherry];rde-1(ne219) V}*
WUM73	*drl-1(vir11)*	*{jyIs8[Ppals-5::GFP; Pmyo-2::mCherry]; rde-1(ne219) V; drl-1(vir11)IV}*
WUM78	*hipr-1(vir12)*	*{jyIs8[Ppals-5::GFP; Pmyo-2::mCherry]; rde-1(ne219) V; hipr-1(vir12)III}*
WUM79	*hipr-1(vir13)*	*{jyIs8[Ppals-5::GFP; Pmyo-2::mCherry]; rde-1(ne219) V; hipr-1(vir13)III}*
WUM80	*hipr-1(vir12);virEx41[Psur-5::hipr-1]*	*{virEx41[Psur-5::hipr-1;Pmyo-2::YFP]; jyIs8[Ppals-5::GFP;P myo-2::mCherry];rde-1(ne219)V; hipr-1(vir12)III}*
WUM81	*hipr-1(vir12);virEx42[Psur-5::hipr-1::mCherry]*	*{virEx42[Psur-5::hipr-1::mCherry;Pmyo-2::YFP]; jyIs8[Ppals-5::GFP;P myo-2::mCherry];rde-1(ne219)V; hipr-1(vir12)III}*
WUM82	*hipr-1(vir12);virEx43[Psur-5::hipr-1(ΔANTH)::mCherry]*	*{virEx43[Psur-5::hipr-1(ΔANTH)::mCherry;Pmyo-2::YFP]; jyIs8[Ppals-5::GFP;P myo-2::mCherry];rde-1(ne219)V; hipr-1(vir12)III}*
WUM83	*hipr-1(vir12);virEx44[Psur-5::hipr-1(ΔCC)::mCherry]*	*{virEx44[Psur-5::hipr-1(ΔCC)::mCherry;Pmyo-2::YFP]; jyIs8[Ppals-5::GFP;P myo-2::mCherry];rde-1(ne219)V; hipr-1(vir12)III}*
WUM84	*hipr-1(vir12);virEx45[Psur-5::hipr1(ΔTHATCH)::mCherry]*	*{virEx45[Psur-5::hipr-1(ΔTHATCH)::mCherry;Pmyo-2::YFP]; jyIs8[Ppals-5::GFP;P myo-2::mCherry];rde-1(ne219)V; hipr-1(vir12)III}*
WUM85	*hipr-1(vir12);virEx46[Psur-5::hipr-1(ΔCHC)::mCherry]*	*{virEx46[Psur-5::hipr-1(ΔCHC)::mCherry;Pmyo-2::YFP]; jyIs8[Ppals-5::GFP;P myo-2::mCherry];rde-1(ne219)V; hipr-1(vir12)III}*
WUM86	*hipr-1(vir12);virEx47[Psur-5::hipr-1(3xY-F)::mCherry]*	*{virEx47[Psur-5::hipr-1(3xY-F)::mCherry;Pmyo-2::YFP]; jyIs8[Ppals-5::GFP;P myo-2::mCherry];rde-1(ne219)V; hipr-1(vir12)III}*
WUM87	*hipr-1(vir12); virEx48[PHIP::RNA1WT-1]*	*{virEx48[PHIP::OrsayRNA1WT-1; Pmyo-2::YFP]; jyIs8[Ppals-5::GFP;Pmyo-2::mCherry];rde-1(ne219) V; hipr-1(vir12)III}*
WUM88	*hipr-1(vir12); virEx49[PHIP::RNA1D601A-1]*	*{virEx49[PHIP::OrsayRNA1D601A-1; Pmyo-2::YFP]; jyIs8[pals-5::GFP;Pmyo-2::mCherry];rde-1(ne219) V; hipr-1(vir12)III}*
WUM89	*hipr-1(vir12);virEx50[Psur-5::hipr-1(Human ANTH):FLAG*	*{virEx50[Psur-5::hipr-1(Human ANTH)::Flag;Pmyo-2::YFP]; jyIs8[Ppals-5::GFP;P myo-2::mCherry];rde-1(ne219)V; hipr-1(vir12)III}*
WUM90	*hipr-1(vir12);virEx51[Psur-5::hipr-1(ΔCHC ΔCC)::mCherry]*	*{virEx51[Psur-5::hipr-1(ΔCHC ΔCC)::mCherry;Pmyo-2::YFP]; jyIs8[Ppals-5::GFP;P myo-2::mCherry];rde-1(ne219)V; hipr-1(vir12)III}*

Plasmid Construction for *hipr-1* Ectopic Expression. To construct the *hipr-1* expression plasmid (*Psur-5p::hipr-1*), the entire *hipr-1* gene was amplified from N2 genomic DNA using primers LS188 and LS195 (*SI Appendix*, Table S1). The PCR product was digested by SacII and NheI and subsequently ligated into the plasmid containing the *sur-5* promoter as previously described (2). To construct the *hipr-1::mCherry* expression plasmid (*Psur-5::hipr-1::mCherry*), the *hipr-1* gene lacking its stop codon was amplified from *Psur-5p::hipr-1* using primers LS188 and LS300 (*SI Appendix*, Table S1). The PCR product was digested by SacII and NotI and then ligated into a plasmid containing the *sur-5* promoter and the mCherry gene with a 15-bp linker, amino acid sequence SGAAA, at the 5′ end of mCherry. Primers for site-directed mutations were generated by Agilent QuikChange Primer Design. Site-directed mutagenesis primers LS396 and LS397, LS398 and LS399, and LS400 and LS401 (*SI Appendix*, Table S1) were used to introduce the desired amino acid substitutions for 3xY-F construct Y111F, Y118F, and Y211F, respectively. Site-directed mutagenesis primers LS447 and LS448 (*SI Appendix*, Table S1) were used to introduce the desired CHC motif deletion of amino acids 307 to 311 into the *Psur-5::hipr-1::mCherry* plasmid. The NEBuilder HiFi DNA Assembly Cloning Kit was used to generate the following three domain deletions in the *Psur-5::hipr-1::mCherry* construct: a 933-bp deletion that deleted parts of exons 1 and 3 and the entire intron 2 and corresponded to a deletion of amino acids 11 to 285 (ANTH domain); a 1,368-bp deletion that deleted exons 4 and 5, introns 3, 4, and 5, and parts of exons 3 and 6 and corresponded to a deletion of amino acids 333 to 527 (coiled-coil domain); and a 999-bp deletion that deleted parts of exons 8 and 9 and the entire intron 8 and corresponded to a deletion of amino acids 713 to 917 (THATCH domain). To generate the *Psur-5::hipr-1::mCherry* plasmid with a deletion of both the CHC motif and coiled-coil domain, site-directed mutagenesis primers LS447 and LS448 (*SI Appendix*, Table S1) were used to introduce the CHC motif deletion of amino acids 307 to 311 into the *Psur-5::hipr-1::mCherry* plasmid that contained a deletion of amino acids 333 to 527 (coiled-coil domain).

To construct the human HIP1 ANTH domain expression construct in the *C. elegans* HIPR-1 expression plasmid, *C. elegans* HIPR-1 complementary DNA was reverse-transcribed, PCR-amplified using primers LS188 and LS195, and then cloned into the *Psur-5* expression vector. The corresponding human HIP1 ANTH domain (primers HJ 454 and HJ 455) and the *C. elegans* HIPR-1 backbone (primers HJ 456 and HJ 457) were PCR-amplified with an ∼20-nt overlapping region and FLAG-tagged at the C terminus. The resulting PCR fragments were gel-purified and assembled with the *Psur-5* expression vector through the NEBuilder HiFi DNA Assembly Kit according to the manufacturer's protocol. Each plasmid sequence was confirmed by Sanger sequencing.

Generating Transgenic Animals Transcomplemented with Plasmids Encoding HIPR-1. For rescue of *hipr-1(vir12)* and *hipr-1(vir13)*, an expression plasmid containing the *hipr-1* gene was injected into the mutant strain at a concentration of 5 ng/μL, along with 5 ng/μL of *Pmyo-2::YFP* as a transgenic marker and 100 ng/μL of a 2-log DNA ladder (New England Biolabs) to help establish the array. For rescue experiments in *hipr-1(vir12)* with HIPR-1::mCherry or HIPR-1::mCherry(ΔCC) mutant constructs, the expression plasmid containing either construct was injected into the mutant strain at a concentration of 5 ng/μL, along with 5 ng/μL of *Pmyo-2::YFP* as a transgenic marker and 100 ng/μL of a 2-log DNA ladder. For rescue experiments in *hipr-1(vir12)* with HIPR-1::mCherry(ΔANTH), HIPR-1::mCherry(ΔCHC), HIPR-1::mCherry(ΔTHATCH), HIPR-1::mCherry(3xY-F), or HIPR-1::mCherry(ΔCHCΔCC) mutant constructs, the expression plasmid was injected into the mutant strain at a concentration of 20 ng/μL, along with 5 ng/μL of *Pmyo-2::YFP* as a transgenic marker and 100 ng/μL of a 2-log DNA ladder. For Orsay virus infection experiments, five stable transgenic array-containing animals were seeded into six-well plates with 20 μL *E. coli* OP50. After 72 h of egg laying, Orsay virus was added to the plates as described above. At 3 dpi, animals were assayed for GFP fluorescence and collected for RNA extraction and qRT-PCR to assay virus replication. For heat induction experiments, five stable transgenic array-containing animals were seeded into six-well plates with 20 μL *E. coli* OP50. After 72 h of egg laying, animals were incubated at 33 °C for 2 h and then maintained at 20 °C for 3 d. At 72 h after heat shock, animals were assayed for GFP fluorescence and collected for RNA extraction and qRT-PCR to assay virus RNA replication.

Phylogenetic Tree Construction. HIP protein amino acid sequences of different species were downloaded from GenBank and aligned by ClustalX (version 2.1). A bootstrap neighbor-joining tree was generated by ClustalX (version 2.1). The number of bootstrap trials was set at 1,000 replicates. The radial tree was exported from TreeView (version 1.6.6).

Epifluorescence Microscopy. The microscopic visual scanning analysis for Orsay virus infection was carried out using a Leica stereo fluorescence microscope. Images of *C. elegans* infections were acquired using a Zeiss Axio Imager M2 inverted fluorescence microscope equipped with a Hamamatsu Flash4.0 CMOS camera for fluorescence. Young adult to adult *C. elegans* animals were anesthetized with 1 mM levamisole and then put on a 2% dry agarose pad with a coverslip (5 by 5 cm) on top. Images were acquired from both fluorescence channels and bright-field channels.

Cell Culture, Knockout Cell Line Generation, and Virus Infection. A549 cells were obtained from the Michael Diamond laboratory. Cells were maintained in Dulbecco's modified Eagle's medium (DMEM) with 25 mM Hepes, 2 mM L-glutamine, 1× nonessential amino acids, 10% fetal bovine serum (FBS), and 100 U/mL antibiotics (penicillin and streptomycin). Hap1 cells were obtained from Horizon and cultured in Iscove's modified Dulbecco's medium with 10% FBS and 100 U/mL antibiotics. HeLa cells were obtained from ATCC and cultured in DMEM with 10% FBS and 100 U/mL antibiotics. A549 cells were transduced by lentiviruses that express the corresponding sgRNA (*SI Appendix*, Table S1) and Cas9 protein. Transduced cells were passaged 2 d later and then selected with 2 μg/mL puromycin for 7 d. Cells were passaged once during this selection. Clonal selection was performed through limiting dilution in 96-well plates. After 2 wk, single-cell clones were picked and expanded in 24-well plates. The desired genome editing was identified by a restriction enzyme digestion-based genome typing assay and the ablation of protein expression was confirmed by Western blot with anti-HIP1 monoclonal antibodies 4B10 (Thermo Fisher Scientific) and anti-HIP1R monoclonal antibodies 1E1 (Thermo Fisher Scientific). For infection quantification by fluorescence-activated cell sorting (FACS) assay, cells were seeded 1 d before infection into 96-well plates. Approximately 16 h after seeding, cells were infected by CVB3 at an MOI of 1. One hour after infection, the inoculum was removed and cells were cultured in DMEM with 2% FBS. At 8 h post infection, cells were trypsinized and fixed with 4% paraformaldehyde. Fixed cells were then permeabilized with perm buffer (1 g saponin, 10 mM Hepes, 0.025% sodium azide in 1 L Hank's balanced salt solution) for 15 min. After permeabilization, cells were incubated with primary antibodies for 1 h and then washed twice before incubation with fluorescently conjugated secondary antibodies. After 1 h of secondary antibody incubation, cells were washed three times with perm buffer and then resuspended with 70 μL of FACS buffer P2F (phosphate-buffered saline with 2% FBS). Infected cells were then analyzed and quantified through MACSQuant Analyzer flow cytometer (Miltenyi Biotec). For multistep growth analysis, cells were infected by CVB3 at an MOI of 0.01. One hour after inoculation, cells were washed five times with serum-free DMEM and then cultured in DMEM with 2% FBS. Culture supernatant was collected at times 0, 6, 12, 24, 36, and 48 h post infection. Viruses released in the culture supernatant were titrated on HeLa cells by plaque assay.

Data Availability. All study data are included in the article and *SI Appendix*.

ACKNOWLEDGMENTS. Some strains were provided by the CGC, which is funded by the NIH Office of Research Infrastructure Programs (P40 OD010440). L.E.S.D.P. is supported in part by NSF Graduate Research Fellowship Program Grant DGE-1745038. This project was supported in part by NIH AI134967 (to D.W.) and American Heart Association Grant 18TPA34230015.

1. M. A. Félix *et al*., Natural and experimental infection of *Caenorhabditis* nematodes by novel viruses related to nodaviruses. *PLoS Biol.* **9**, e1000586 (2011).
2. H. Jiang, K. Chen, L. E. Sandoval, C. Leung, D. Wang, An evolutionarily conserved pathway essential for Orsay virus infection of *Caenorhabditis elegans*. *MBio* **8**, e00940-17 (2017).
3. L. E. Sandoval, H. Jiang, D. Wang, The dietary restriction-like gene *drl-1*, which encodes a putative serine/threonine kinase, is essential for Orsay virus infection in *Caenorhabditis elegans*. *J. Virol.* **93**, e01400-18 (2019).
4. S. Sadeghipour, E. J. Bek, P. C. McMinn, Ribavirin-resistant mutants of human enterovirus 71 express a high replication fidelity phenotype during growth in cell culture. *J. Virol.* **87**, 1759–1769 (2013).
5. T. Kobayashi *et al*., A plasmid-based reverse genetics system for animal double-stranded RNA viruses. *Cell Host Microbe* **1**, 147–157 (2007).
6. M. Metzler *et al*., HIP1 functions in clathrin-mediated endocytosis through binding to clathrin and adaptor protein 2. *J. Biol. Chem.* **276**, 39271–39276 (2001).
7. M. Kaksonen, Y. Sun, D. G. Drubin, A pathway for association of receptors, adaptors, and actin during endocytic internalization. *Cell* **115**, 475–487 (2003).
8. A. E. Engqvist-Goldstein *et al*., RNAi-mediated Hip1R silencing results in stable association between the endocytic machinery and the actin assembly machinery. *Mol. Biol. Cell* **15**, 1666–1679 (2004).
9. T. S. Hyun *et al*., HIP1 and HIP1r stabilize receptor tyrosine kinases and bind 3-phosphoinositides via epsin N-terminal homology domains. *J. Biol. Chem.* **279**, 14294–14306 (2004).
10. Y. Sun, M. Kaksonen, D. T. Madden, R. Schekman, D. G. Drubin, Interaction of Sla2p's ANTH domain with PtdIns(4,5)P_2 is important for actin-dependent endocytic internalization. *Mol. Biol. Cell* **16**, 717–730 (2005).
11. I. Gottfried, M. Ehrlich, U. Ashery, HIP1 exhibits an early recruitment and a late stage function in the maturation of coated pits. *Cell. Mol. Life Sci.* **66**, 2897–2911 (2009).
12. D. R. Boettner, H. Friesen, B. Andrews, S. K. Lemmon, Clathrin light chain directs endocytosis by influencing the binding of the yeast Hip1R homologue, Sla2, to F-actin. *Mol. Biol. Cell* **22**, 3699–3714 (2011).
13. J. A. Parker *et al*., Huntingtin-interacting protein 1 influences worm and mouse presynaptic function and protects *Caenorhabditis elegans* neurons against mutant polyglutamine toxicity. *J. Neurosci.* **27**, 11056–11064 (2007).
14. J. F. Winter *et al*., *Caenorhabditis elegans* screen reveals role of PAR-5 in RAB-11-recycling endosome positioning and apicobasal cell polarity. *Nat. Cell Biol.* **14**, 666–676 (2012).
15. A. E. Engqvist-Goldstein, M. M. Kessels, V. S. Chopra, M. R. Hayden, D. G. Drubin, An actin-binding protein of the Sla2/huntingtin interacting protein 1 family is a novel component of clathrin-coated pits and vesicles. *J. Cell Biol.* **147**, 1503–1518 (1999).
16. T. S. Hyun *et al*., Hip1-related mutant mice grow and develop normally but have accelerated spinal abnormalities and dwarfism in the absence of HIP1. *Mol. Cell. Biol.* **24**, 4329–4340 (2004).
17. R. N. Jain *et al*., Hip1r is expressed in gastric parietal cells and is required for tubulovesicle formation and cell survival in mice. *J. Clin. Invest.* **118**, 2459–2470 (2008).
18. K. I. Oravecz-Wilson *et al*., Huntingtin interacting protein 1 mutations lead to abnormal hematopoiesis, spinal defects and cataracts. *Hum. Mol. Genet.* **13**, 851–867 (2004).
19. D. S. Rao *et al*., Huntingtin interacting protein 1 is a clathrin coat binding protein required for differentiation of late spermatogenic progenitors. *Mol. Cell. Biol.* **21**, 7796–7806 (2001).
20. M. Metzler *et al*., Disruption of the endocytic protein HIP1 results in neurological deficits and decreased AMPA receptor trafficking. *EMBO J.* **22**, 3254–3266 (2003).
21. S. V. Bradley *et al*., Degenerative phenotypes caused by the combined deficiency of murine HIP1 and HIP1r are rescued by human HIP1. *Hum. Mol. Genet.* **16**, 1279–1292 (2007).
22. I. G. Mills *et al*., Huntingtin interacting protein 1 modulates the transcriptional activity of nuclear hormone receptors. *J. Cell Biol.* **170**, 191–200 (2005).
23. H. M. Ames *et al*., Huntingtin-interacting protein 1 phosphorylation by receptor tyrosine kinases. *Mol. Cell. Biol.* **33**, 3580–3593 (2013).
24. K. E. Coller *et al*., RNA interference and single particle tracking analysis of hepatitis C virus endocytosis. *PLoS Pathog.* **5**, e1000702 (2009).
25. O. Ilnytska *et al*., Enteroviruses harness the cellular endocytic machinery to remodel the host cell cholesterol landscape for effective viral replication. *Cell Host Microbe* **14**, 281–293 (2013).
26. S. R. Radoshitzky *et al*., siRNA screen identifies trafficking host factors that modulate alphavirus infection. *PLoS Pathog.* **12**, e1005466 (2016).
27. G. Minevich, D. S. Park, D. Blankenberg, R. J. Poole, O. Hobert, CloudMap: A cloud-based pipeline for analysis of mutant genome sequences. *Genetics* **192**, 1249–1269 (2012).
28. V. Legendre-Guillemin *et al*., HIP1 and HIP12 display differential binding to F-actin, AP2, and clathrin. Identification of a novel interaction with clathrin light chain. *J. Biol. Chem.* **277**, 19897–19904 (2002).
29. T. M. Newpher, S. K. Lemmon, Clathrin is important for normal actin dynamics and progression of Sla2p-containing patches during endocytosis in yeast. *Traffic* **7**, 574–588 (2006).
30. R. O. McCann, S. W. Craig, Functional genomic analysis reveals the utility of the I/LWEQ module as a predictor of protein:actin interaction. *Biochem. Biophys. Res. Commun.* **266**, 135–140 (1999).
31. M. A. Senetar, S. J. Foster, R. O. McCann, Intrasteric inhibition mediates the interaction of the I/LWEQ module proteins Talin1, Talin2, Hip1, and Hip12 with actin. *Biochemistry* **43**, 15418–15428 (2004).
32. E. ter Haar, S. C. Harrison, T. Kirchhausen, Peptide-in-groove interactions link target proteins to the beta-propeller of clathrin. *Proc. Natl. Acad. Sci. U.S.A.* **97**, 1096–1100 (2000).
33. S. K. Mishra *et al*., Clathrin- and AP-2-binding sites in HIP1 uncover a general assembly role for endocytic accessory proteins. *J. Biol. Chem.* **276**, 46230–46236 (2001).

34. E. E. Wanker *et al*., HIP-I: A huntingtin interacting protein isolated by the yeast two-hybrid system. *Hum. Mol. Genet.* **6**, 487–495 (1997).
35. M. A. Kalchman *et al*., HIP1, a human homologue of *S. cerevisiae* Sla2p, interacts with membrane-associated huntingtin in the brain. *Nat. Genet.* **16**, 44–53 (1997).
36. C. Y. Chen, F. M. Brodsky, Huntingtin-interacting protein 1 (Hip1) and Hip1-related protein (Hip1R) bind the conserved sequence of clathrin light chains and thereby influence clathrin assembly in vitro and actin distribution in vivo. *J. Biol. Chem.* **280**, 6109–6117 (2005).
37. V. Legendre-Guillemin *et al*., Huntingtin interacting protein 1 (HIP1) regulates clathrin assembly through direct binding to the regulatory region of the clathrin light chain. *J. Biol. Chem.* **280**, 6101–6108 (2005).
38. J. A. Ybe, S. Mishra, S. Helms, J. Nix, Crystal structure at 2.8 Å of the DLLRKN-containing coiled-coil domain of huntingtin-interacting protein 1 (HIP1) reveals a surface suitable for clathrin light chain binding. *J. Mol. Biol.* **367**, 8–15 (2007).
39. C. W. Gourlay *et al*., An interaction between Sla1p and Sla2p plays a role in regulating actin dynamics and endocytosis in budding yeast. *J. Cell Sci.* **116**, 2551–2564 (2003).
40. M. G. Ford *et al*., Simultaneous binding of PtdIns(4,5)P_2 and clathrin by AP180 in the nucleation of clathrin lattices on membranes. *Science* **291**, 1051–1055 (2001).
41. T. Itoh *et al*., Role of the ENTH domain in phosphatidylinositol-4,5-bisphosphate binding and endocytosis. *Science* **291**, 1047–1051 (2001).
42. G. Odorizzi, M. Babst, S. D. Emr, Fab1p PtdIns(3)P 5-kinase function essential for protein sorting in the multivesicular body. *Cell* **95**, 847–858 (1998).
43. A. Kihara, T. Noda, N. Ishihara, Y. Ohsumi, Two distinct Vps34 phosphatidylinositol 3-kinase complexes function in autophagy and carboxypeptidase Y sorting in *Saccharomyces cerevisiae*. *J. Cell Biol.* **152**, 519–530 (2001).
44. R. S. Kamath *et al*., Systematic functional analysis of the *Caenorhabditis elegans* genome using RNAi. *Nature* **421**, 231–237 (2003).